Molecular Cell, Volume *28*

Supplemental Data

Structural Basis and Mechanism of Autoregulation in 3-Phosphoinositide-Dependent Grp1 Family Arf GTPase Exchange Factors

Jonathan P. DiNitto, Anna Delprato, Meng-Tse Gabe Lee, Thomas C. Cronin, Shaohui Huang, Adilson Guilherme, Michael P. Czech, and David G. Lambright

Table S1. Catalytic Efficiency of Grp1 Family Constructs and Complexes

ΔN17Arf1			
Protein	**Construct**	**k_{cat}/K_m (10^4 $M^{-1}s^{-1}$)**	**k_{cat}/K_m (Arb. Units)**
Grp1	Sec7	8.0 ± 1.3	78 ± 12
	Sec7-PH	7.6 ± 0.43	74 ± 4.1
	Sec7-PH-pb	0.1 ± 0.003	1.0 ± 0.1
	hr-Sec7-PH	4.7 ± 0.57	45 ± 5.5
	hr-Sec7-PH-pb	0.25 ± 0.093	2.4 ± 0.9
ARNO	Sec7	33 ± 1.4	230 ± 9.7
	Sec7-PH	16 ± 0.72	110 ± 4.9
	Sec7-PH-pb	0.15 ± 0.004	1.0 ± 0.1
	hr-Sec7-PH	2.3 ± 0.06	16 ± 0.4
	hr-Sec7-PH-pb	0.082 ± 0.004	0.56 ± 0.1
Cytohesin-1	Sec7	18 ± 0.78	89 ± 3.8
	Sec7-PH	14 ± 0.91	73 ± 4.4
	Sec7-PH-pb	0.2 ± 0.01	1.0 ± 0.1
	hr-Sec7-PH	3.2 ± 0.06	16 ± 0.3
	hr-Sec7-PH-pb	0.061 ± 0.024	0.3 ± 0.1
Grp1-Grsp1 complex (-IP_4)	hr-Sec7-PH/FERM-hr	3.5 ± 0.41	36 ± 4.2
	hr-Sec7-PH-pb/FERM-hr	0.098 ± 0.030	1.0 ± 0.1
Grp1-Grsp1 complex (+IP_4)	hr-Sec7-PH/FERM-hr	5.0 ± 0.30	11 ± 3.0
	hr-Sec7-PH-pb/FERM-hr	0.47 ± 0.038	1.0 ± 0.1
ΔN12Arf6			
Grp1	Sec7	0.28 ± 0.029	24 ± 2.5
	Sec7-PH	0.64 ± 0.025	54 ± 2.1
	Sec7-PH-pb	0.012 ± 0.001	1.0 ± 0.1
	hr-Sec7-PH	0.7 ± 0.029	60 ± 2.4
	hr-Sec7-PH-pb	0.013 ± 0.001	1.1 ± 0.1
ARNO	Sec7	6 ± 0.19	32 ± 1.0

	Sec7-PH	4.2 ± 0.07	22 ± 3.8
	Sec7-PH-pb	0.19 ± 0.015	1.0 ± 0.1
	hr-Sec7-PH	1.2 ± 0.099	6.5 ± 0.5
	hr-Sec7-PH-pb	0.073 ± 0.008	0.4 ± 0.1
Cytohesin-1	Sec7	3 ± 0.46	32 ± 4.8
	Sec7-PH	3.2 ± 0.11	34 ± 1.2
	Sec7-PH-pb	0.095 ± 0.005	1.0 ± 0.1
	hr-Sec7-PH	0.95 ± 0.035	10 ± 0.3
	hr-Sec7-PH-pb	0.032 ± 0.003	0.3 ± 0.1
Grp1-Grsp1 complex (-IP_4)	hr-Sec7-PH/FERM-hr	0.43 ± 0.002	12 ± 0.1
	hr-Sec7-PH-pb/FERM-hr	0.036 ± 0.003	1.0 ± 0.1
Grp1-Grsp1 complex (+IP_4)	hr-Sec7-PH/FERM-hr	0.49 ± 0.005	14 ± 0.1
	hr-Sec7-PH-pb/FERM-hr	0.036 ± 0.001	1.0 ± 0.1

hr, heptad repeats; Sec7, Sec7 domain; PH, Pleckstrin homology domain; pb, polybasic region; IP_4, Ins(1,3,4,5)P_4.

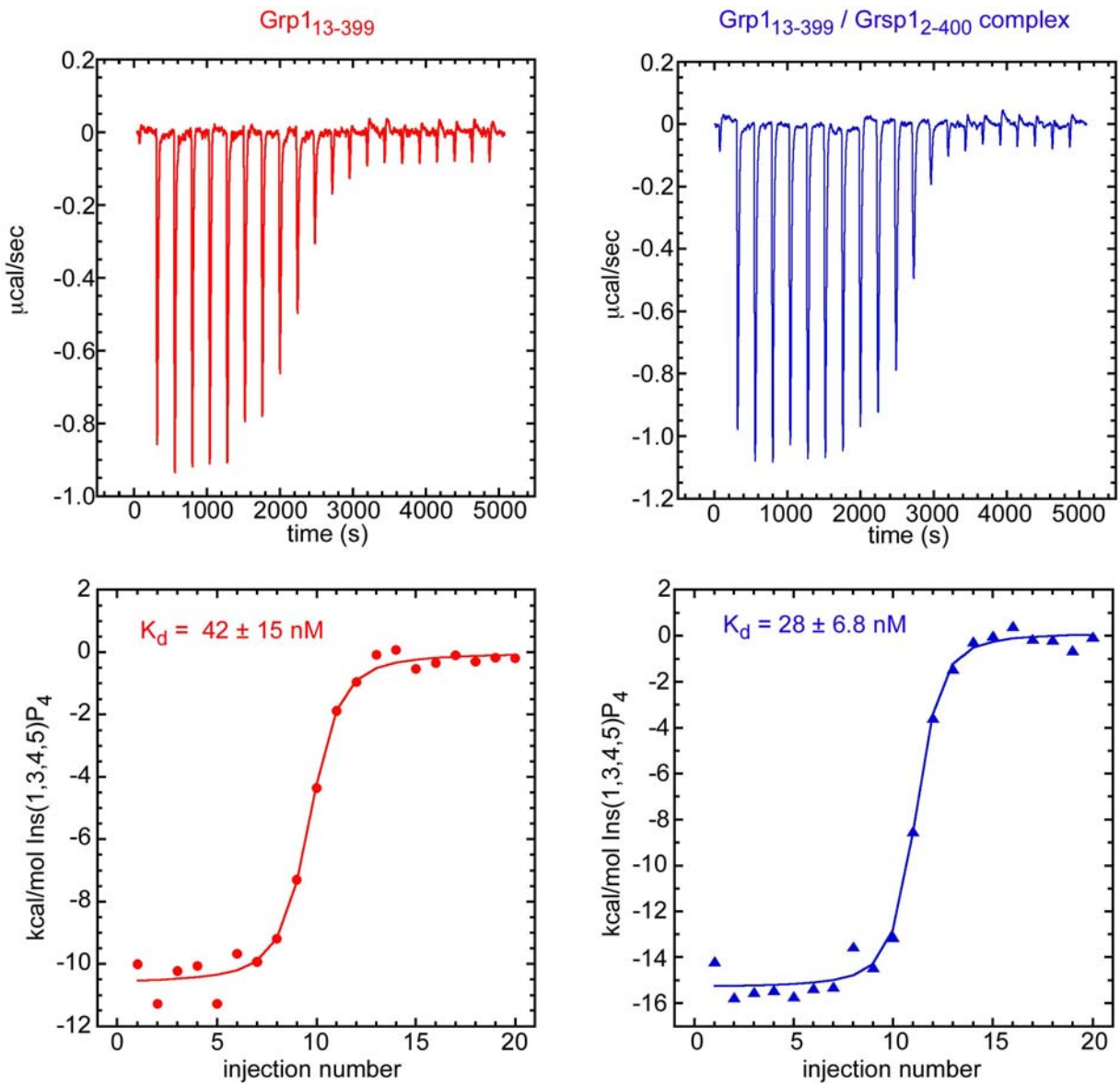

Figure S1. Affinity of Ins(1,3,4,5)P_4 for Grp1 and the Grp1-Grsp1 Complex Analyzed by Isothermal Titration Microcalorimetry

Samples of $Grp1_{13-399}$ (10 µM) or the $Grp1_{13-399}$-$Grsp1_{2-400}$ complex (10 µM) were titrated with Ins(1,3,4,5)P_4. Raw data were corrected for baseline drift and the total heat released during each injection determined by integrating over the injection period. Dissociation constants (K_d) were determined by fitting to a 1:1 binding model as described in Cronin et al. (2004) *EMBO J.* **23**: 3711-3720.

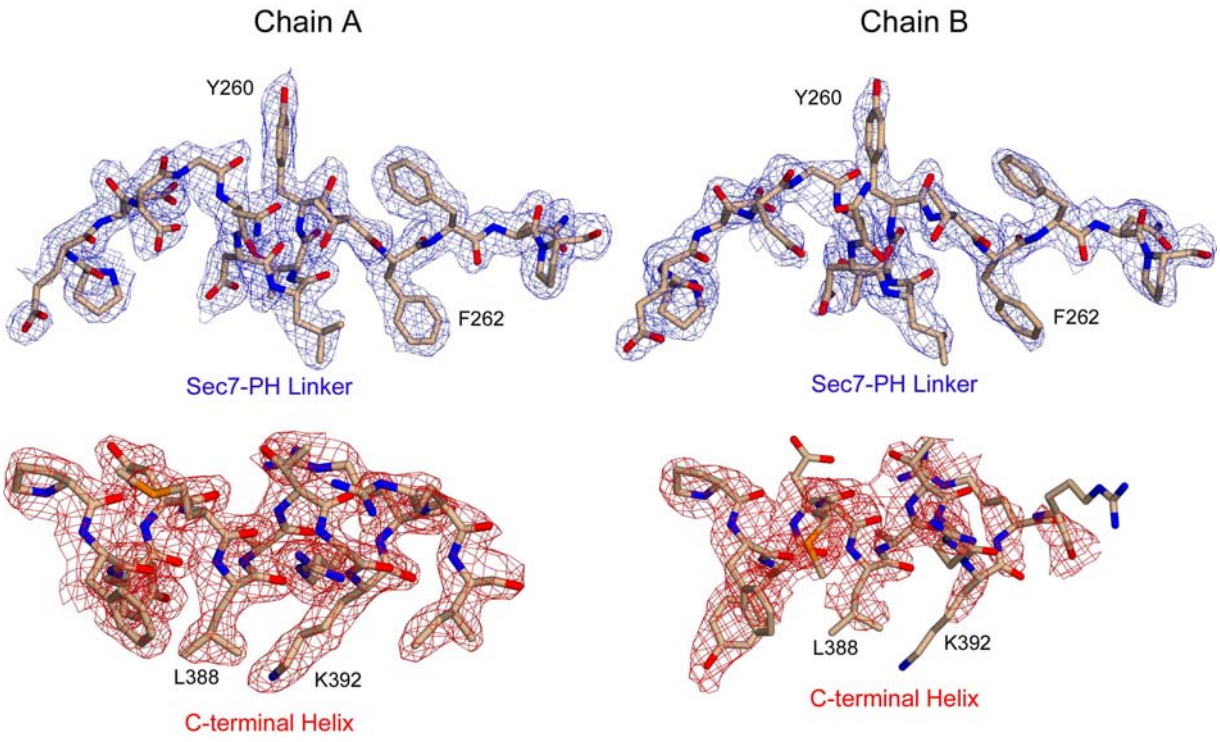

Figure S2. Experimental Electron Density for Functionally Relevant Regions of the Grp1$_{63-399}$ K68A/H260Y Mutant

σA weighted $2wF_o$-DF_c maps were calculated with phases derived from a 3 wavelength MAD experiment and improved by solvent flipping. The maps include data from 20-1.95 Å and are contoured at 1.0 σ.

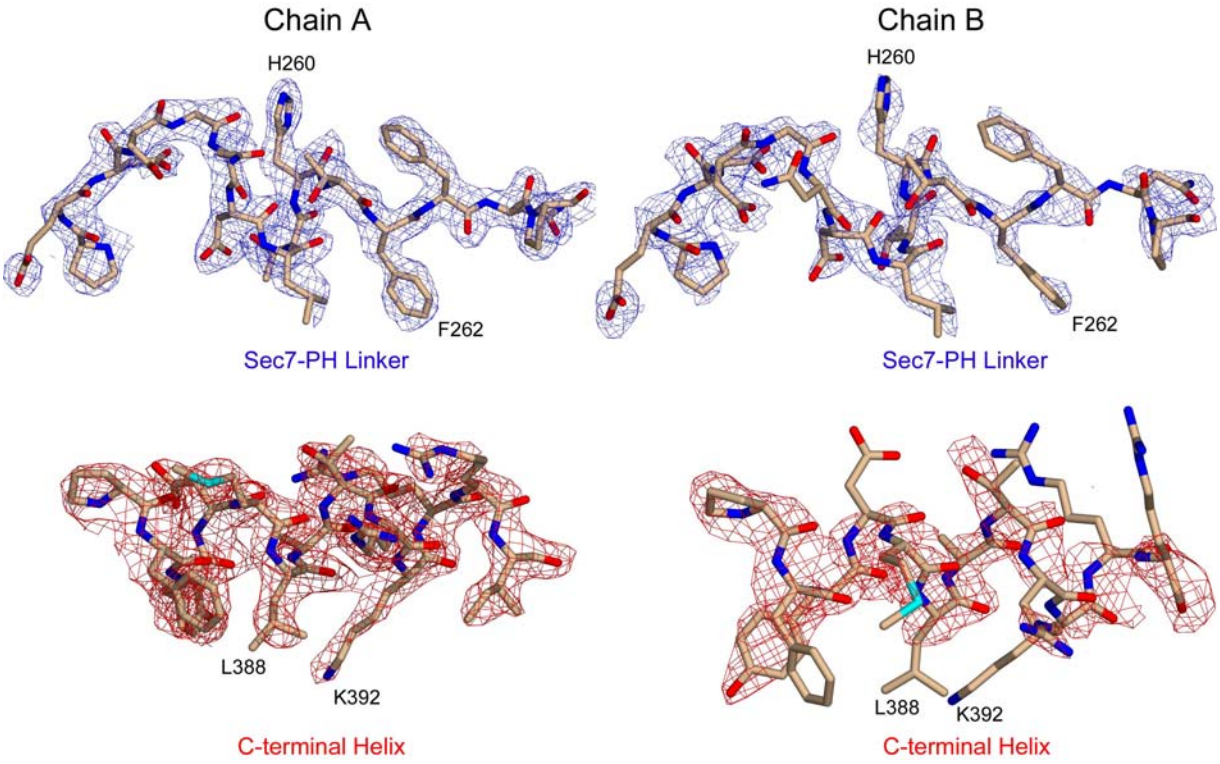

Figure S3. Simulated Annealing Omit Maps for Functionally Relevant Regions of the Grp1$_{63-399}$ K68A Mutant

The final refined model is shown with the electron density from σA weighted $2F_o$-F_c maps following simulated annealing with the linker or C-terminal helix omitted. Maps include data from 20.0-2.0 Å and are contoured at 1.0 σ.

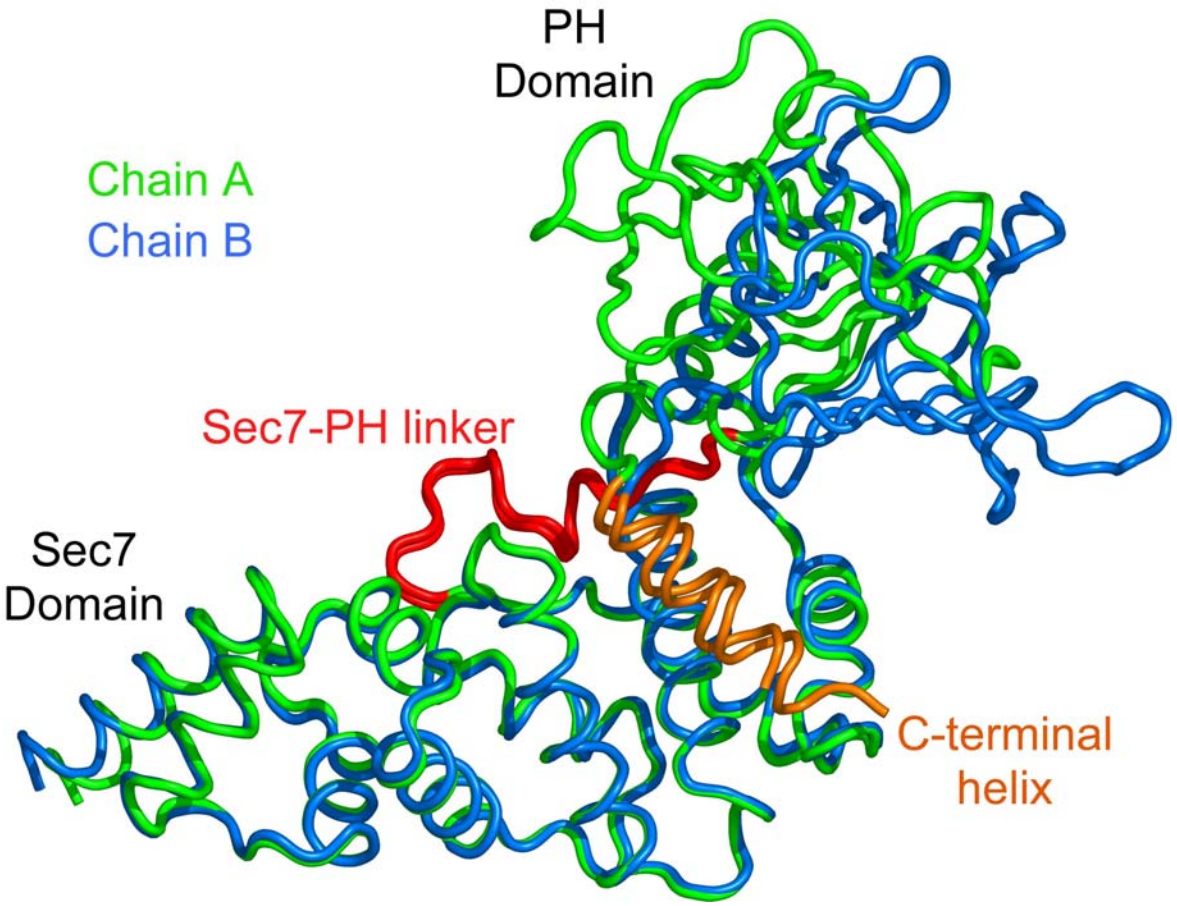

Figure S4. Comparison of the Two Molecules in the Asymmetric Unit Following Superposition of the Sec7 Domains

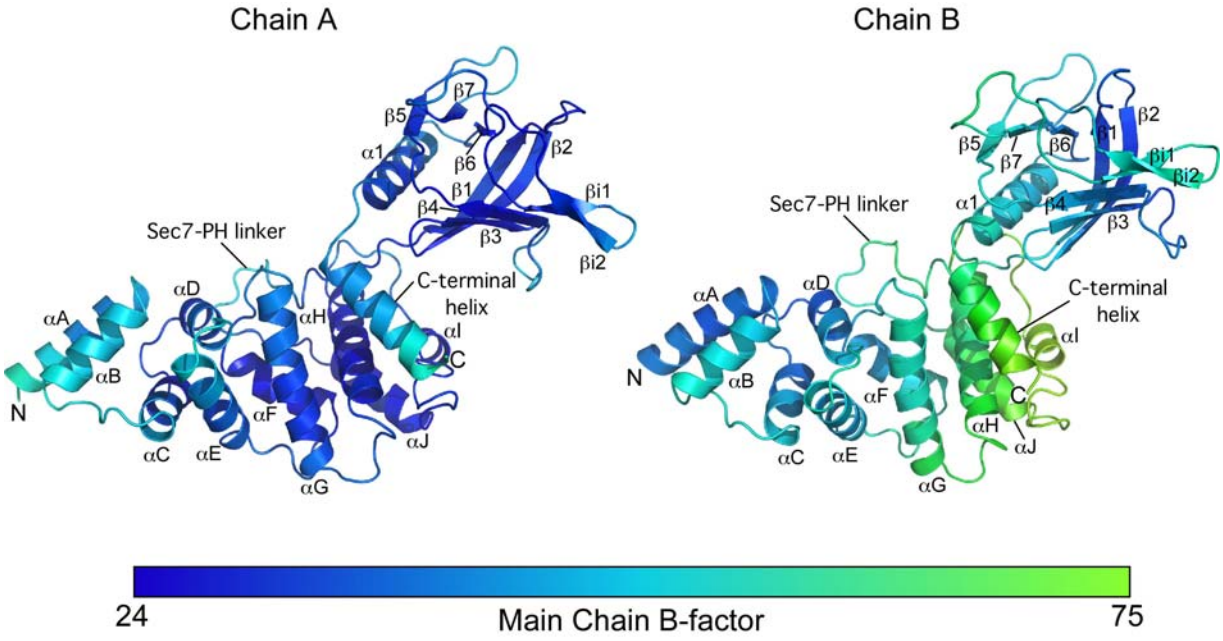

Figure S5. B Factors for Main-Chain Atoms of Molecule A and B in the Asymmetric Unit for Native Crystals of Grp1$_{63–399}$

The view and orientation is similar to Figure 2. B-factors from the main chain atoms of the refined structure are mapped to the ribbon representation with color gradient proportional to the B-factor. The overall B-factor is higher in chain B than in chain A. The figure was generated with PyMol (Delano Scientific).

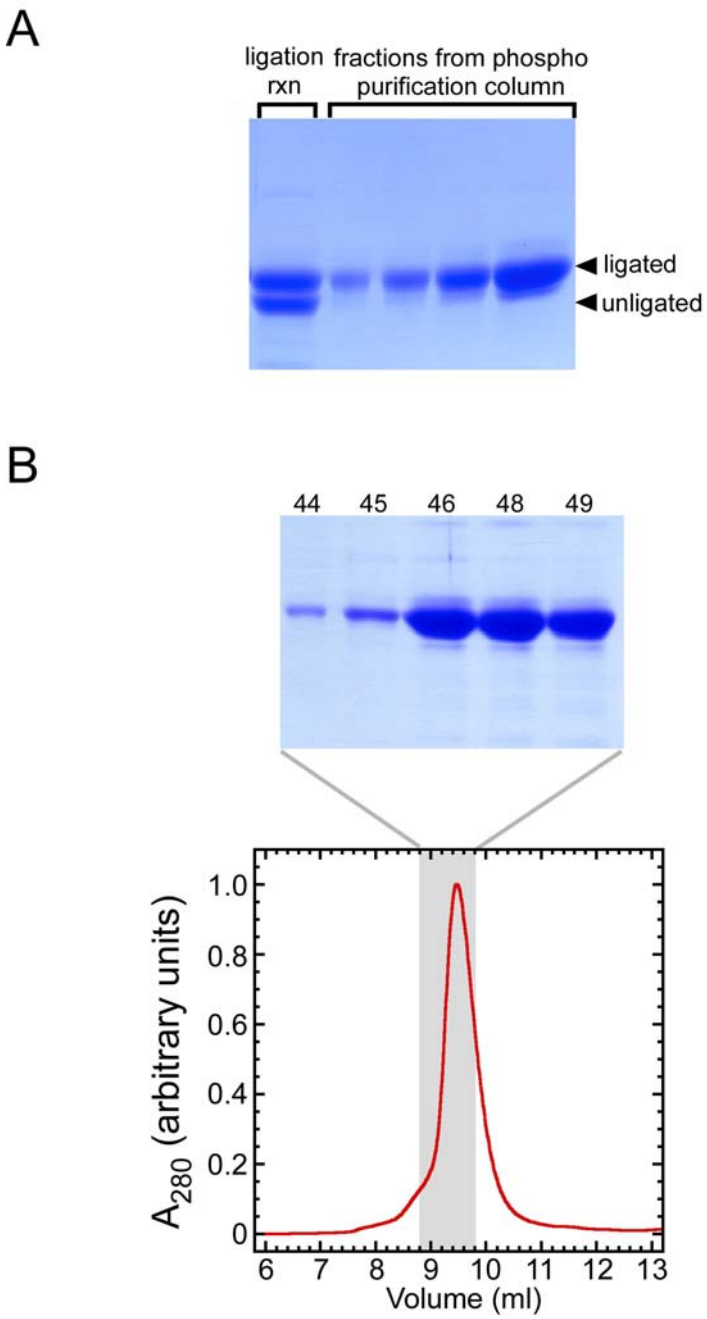

Figure S6. Purification of Phosphorylated Cytohesin-1 R378C Following Intein-Mediated Ligation

(A) SDS-PAGE gel of fractions from a phosphopurification column (Qiagen).

(B) Elution profile from Superdex-75 column. Shown above the elution profile are fractions analyzed by SDS-PAGE.

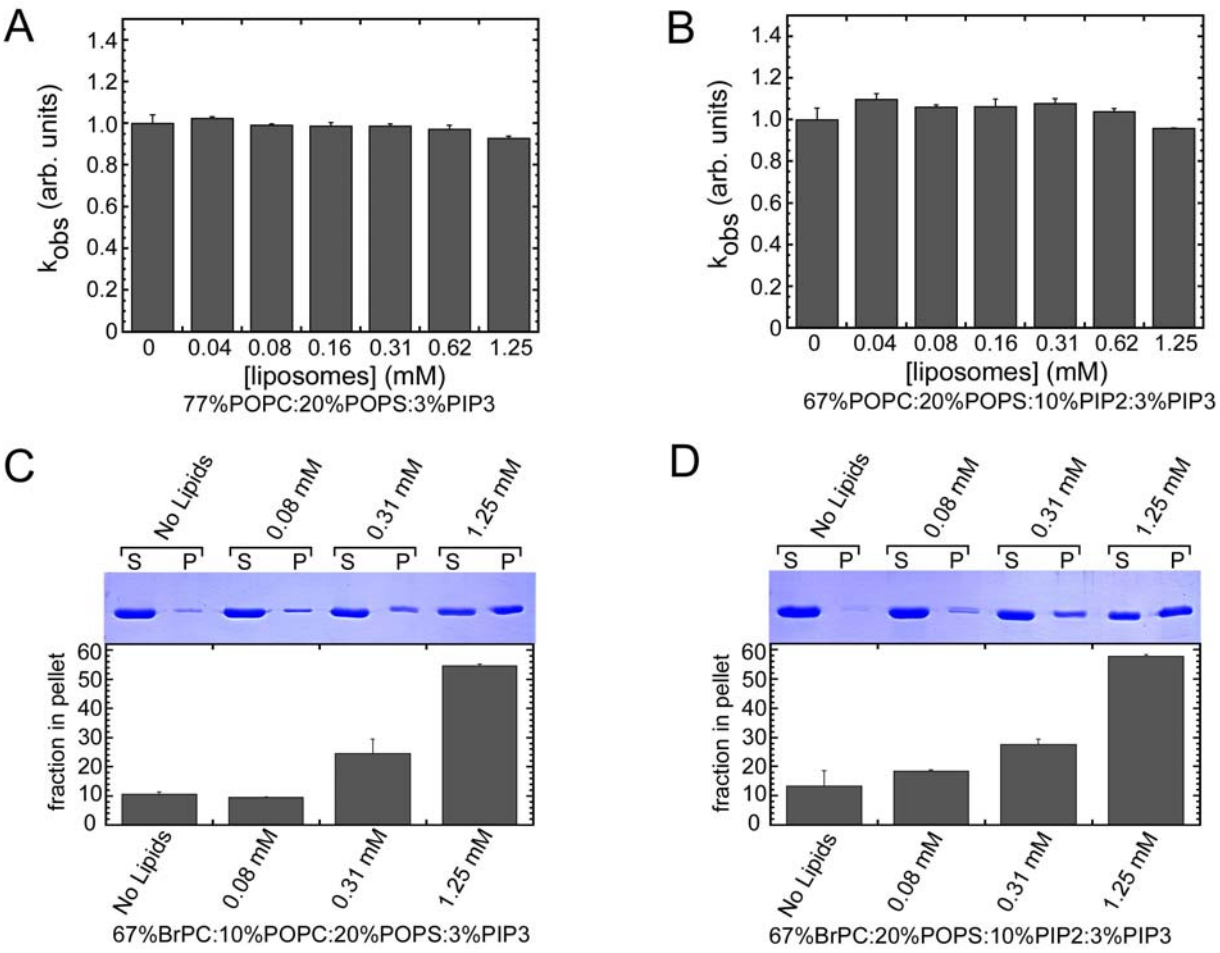

Figure S7. Effect of Liposomes on the ΔN12Arf6 Exchange Activity of Grp1$_{63–399}$
(A and B) The catalytic activity of autoinhibited Grp1$_{63-399}$ (2 μM) was measured as a function of liposome concentration.
(C and D) Co-sedimentation of Grp1$_{63-399}$ with liposomes under the same conditions as in panels A and B. SDS-PAGE gels were quantified using GelEval 1.1. Plots below the gels represent the mean and deviation of the background corrected integrated band intensity for 2 independent determinations.

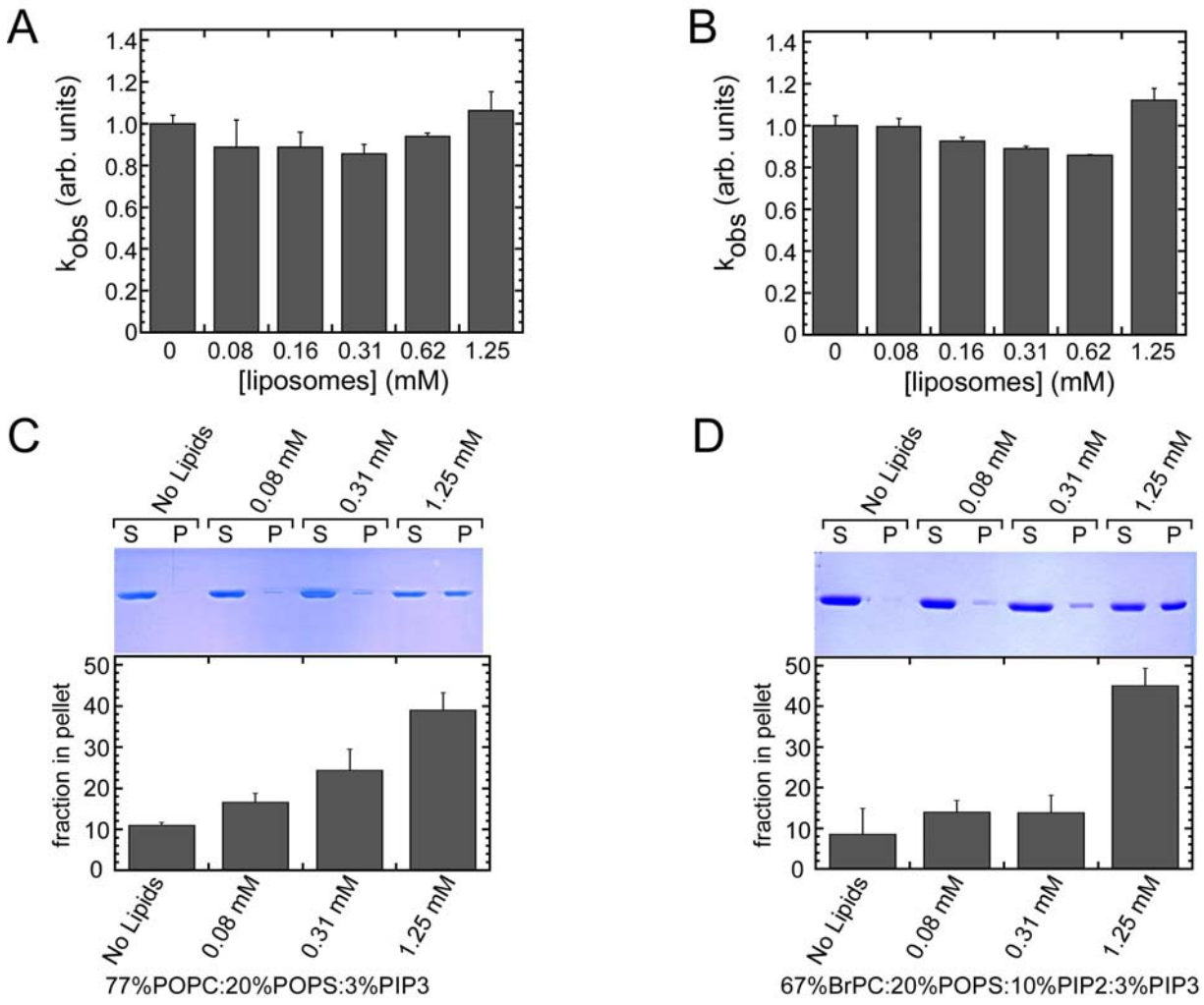

Figure S8. Effect of Liposomes on the ΔN12Arf6 Exchange Activity of Cytohesin-$1_{53–398}$
(A and B) Catalytic activity of autoinhibited Cytohesin-1_{53-398} (2 μM) as a function of liposome concentration.
(C and D) Co-sedimentation of Cytohesin-1_{53-398} with liposomes under the same conditions as in panels A and B. SDS-PAGE gels were quantified using GelEval 1.1. Plots below the gels represent the mean and deviation of the background corrected integrated band intensity for 2 independent determinations.

Experimental Procedures for Figures S7 and S8

Exchange Assays for Liposome Partitioning Experiments

The kinetics of nucleotide exchange were monitored using the decrease in fluorescence accompanying release of mant-GDP from Arf GTPases. Exchange reactions were initiated by the addition of mant-GDP loaded ΔN17Arf1 or ΔN12Arf6 (1 μM unless otherwise indicated) and varying concentrations of exchange factor in the presence of 250 μM GppNHp. Data were collected using a Saphire multimode microplate spectrophotometer (Tecan). Samples were excited at 360 nm and the emission detected at 440 nm. Observed pseudo first order rate constants (k_{obs}) were extracted from a nonlinear least-squares fit to the exponential function

$$I(t) = (I_0 - I_\infty) \exp(-k_{obs}\, t) + I_\infty$$

where I(t) is the emission intensity as a function of time and I_0 and I_∞ are the initial and final emission intensities, respectively. The catalytic efficiency, k_{cat}/K_m, was obtained from the slope of a linear least squares fit to

$$k_{obs} = (k_{cat}/K_m)\,[\text{Sec7}] + k_{intr}$$

where k_{intr} is the intrinsic rate constant for mant-GDP release.

Liposome Partitioning

Phospholipids (Avanti) and phosphoinositides (Cell Signals) were dissolved in chloroform, mixed in the desired molar ratios using a Drummond pipettor, dried by evaporation, and rehydrated in 50 mM Tris, pH 8.0, 150 mM KCl, 1 mM $MgCl_2$. Small unilamellar vesicles (SUVs) were prepared by rapid freeze-thaw cycling in liquid nitrogen (10 cycles) followed by bath sonication for 30 minutes. Proteins were added to a final concentration of 2 μM and the resulting mixtures incubated for 1 hour at 25°C followed by centrifugation at 100,000 g for 1 hr at 25°C. Pellets were redissolved in an equivalent volume. Samples were analyzed by SDS-PAGE with Coomassie Blue staining and quantified using the GelEval 1.1.